

# Spectral properties of massless and massive quarks coupled with massive boson at finite temperature

Masakiyo Kitazawa,<sup>1,\*</sup> Teiji Kunihiro,<sup>2,†</sup> Kazuya Mitsutani,<sup>2,‡</sup> and Yukio Nemoto<sup>3,§</sup>

<sup>1</sup> *Department of Physics, Osaka University, Toyonaka, Osaka 560-0043, Japan*

<sup>2</sup> *Yukawa Institute for Theoretical Physics, Kyoto University, Kyoto, 606-8502, Japan*

<sup>3</sup> *Department of Physics, Nagoya University, Nagoya, 464-8602, Japan*

(Dated: February 9, 2008)

We study the properties of massless and massive quarks coupled with a scalar and pseudoscalar boson at finite temperature in Yukawa models at the one-loop order. The behavior of the spectral function and the pole structure of the propagator are analyzed as functions of temperature  $T$  and the quark mass  $m_f$ . It is shown that the three-peak structure of the spectral function found in a previous work for massless quarks is formed at temperatures comparable to the boson mass even for finite  $m_f$ , but gradually ceases to exist as  $m_f$  becomes larger. We identify the three poles of the quark propagator corresponding to the collective excitations of the quark in the complex energy plane. It is shown that the three trajectories made by the poles along with a variation of  $T$  undergo a structural rearrangement at a critical quark mass when  $m_f$  is increased. This suggests that the physics content of the collective quark excitations is changed in a drastic way at this point. The results are nicely accounted for with the notion of the level mixing induced by a resonant scattering of the massive boson with quarks and holes of thermally excited anti-quarks.

PACS numbers: 11.10.Wx, 11.30.Rd, 12.38.Bx, 12.38.Mh, 25.75.Nq

## I. INTRODUCTION

Hadronic matter undergoes deconfinement and chiral phase transitions to the quark-gluon plasma (QGP) phase at finite temperature ( $T$ ). Owing to the asymptotic freedom of QCD, the QGP phase at asymptotically high  $T$  is composed of approximately free quarks and gluons, where a perturbation expansion is valid. It is known that the leading order of such an expansion is obtained with the hard thermal loop (HTL) approximation [1] which enables us to calculate the quark and gluon propagators in a gauge-invariant way. One of notable features obtained in the HTL approximation is that the quarks and gluons have collective excitations with mass gaps called thermal masses proportional to  $gT$ , where  $g$  is the gauge coupling [2, 3].

Recently, properties of the QGP phase near the critical temperature ( $T_c$ ) acquire much interest. Measurements of the elliptic flow of hadrons in the heavy-ion collisions were made at the Relativistic Heavy Ion Collider (RHIC), and the subsequent phenomenological analyses have shown that the experimental results are in remarkably good agreement with the predictions of the ideal fluid dynamics [4]. This result suggests that the created matter is a strongly coupled system. The present paper is concerned with the properties of quarks in such a system, which constitute the basic degrees of freedom of the created matter in the deconfined phase together

with gluons. We explore possible quasi-particle picture of quarks in the QGP phase near  $T_c$ .

It is not a priori clear whether quarks manifest themselves as well-defined quasi-particles in such a nonperturbative region; quasi-particles in Landau's sense correspond to peaks with a small width in the spectral function with relevant quantum numbers. In the phenomenological side, the success of the recombination model to describe the RHIC data [5] tells us that the quark quasi-particles play an important role in some stage of the evolution of the created matter in RHIC. In the theoretical side, a recent lattice QCD simulation [6] indicates the existence of the quasi-particles of quarks with small decay width, though in quenched approximation. Quasi-particle properties of quarks are also obtained in a strong coupling gauge theory based on the Schwinger-Dyson equation at finite  $T$ , unless the coupling is too large [7]. The quarks thus will exist as one of the basic degrees of freedom of the system even near  $T_c$ , and hence revealing their nature will provide us with important information necessary to understand the nature of QGP phase at the strong coupling.

To study the quasi-particle properties of quarks around  $T_c$ , we notice the possible existence of hadronic excitations even in the QGP phase near  $T_c$  [8, 9]. The numerical results in lattice QCD suggest the existence of such states in the heavy-quark sector [10]. The existence of the mesonic excitations in the light-quark sector was also predicted as being the soft modes associated with the chiral transition [8]. If such bosonic modes are light enough so that many particles are thermally excited in the system, they can in turn strongly affect excitation spectra of quarks. Part of the authors in the present paper (M.K., T.K. and Y.N.) considered such possibility in Refs. [11, 12]. They first evaluated the effect of the

\*Electronic address: kitazawa@phys.sci.osaka-u.ac.jp

†Electronic address: kunihiro@yukawa.kyoto-u.ac.jp

‡Electronic address: kazuya@yukawa.kyoto-u.ac.jp

§Electronic address: nemoto@hken.phys.nagoya-u.ac.jp

chiral soft modes on quarks in a chiral effective model [11] where the soft modes are described as composite bosons composed of a quark and anti-quark: An interesting result obtained there was that there appears a novel three-peak structure in the quark spectral function near but above  $T_c$ . It was also pointed out that the coupling of quarks with bosonic excitations which have a finite mass and small width is essential for the formation of the multi-peak structure. In fact, it was later shown [12] that the three-peak structure in the quark spectral function emerges at intermediate temperatures even in the Yukawa models composed of a massless fermion and a massive boson with a zero width, irrespective whether the boson is of scalar, pseudoscalar, vector or axial-vector type.

In the previous work [11, 12], the massless quarks were exclusively adopted to explore the effects of the soft modes on the quarks in the most ideal case where the chiral symmetry is exact. In reality, the quarks in the QGP phase near  $T_c$  should have current or dynamical Dirac masses which may be as large as the order of  $T_c$  and may not be negligible. In this paper, we examine how the finite Dirac mass of the quark modifies the spectral properties, employing the Yukawa model composed of a massive quark with a small mass and a massive boson. We shall show that the three-peak structure found in Ref. [12] survives even with finite  $m_f$ , although one of the three peaks is gradually suppressed as  $m_f$  is larger.

In addition to the analysis of the spectral function, we newly explore the pole structure of the quark propagator in the complex-energy plane and their residues. We show that there always exist three poles corresponding to the peaks in the spectral function in the complex-energy plane at finite  $T$ . It is found that the trajectories of these poles along with an increase of  $T$  undergoes a structural change at a critical value of  $m_f$  as  $m_f$  is increased. We give a physical interpretation for these properties of the quark spectrum at finite  $m_f$  adapting the notion of the level repulsion in quantum mechanics.

This paper is organized as follows. In Secs. II-IV, we study the spectral properties of the quark coupled with a scalar boson. After introducing the Yukawa model in Sec. II, we present the numerical result for the quark spectral function in Sec. III and the pole structure of the propagator in Sec. IV. We then discuss the spectral properties of the quark coupled with a pseudoscalar boson in Sec. V. In Sec. VI, we elucidate the physical mechanism of the  $m_f$ -dependence of the quark spectrum. Section VII is devoted to the summary and some discussions. In Appendix A, we present the renormalization procedure of the quark propagator using the subtracted dispersion relations. In Appendix B, we introduce an analytic toy model and elucidate that a two-peak structure of the quark self-energy is essential for the appearance of the three-peak structure in the quark spectrum. To simplify the analysis, we restrict the following calculations to zero momentum to concentrate on the  $T$  dependence.

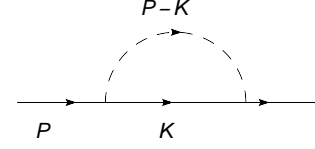


FIG. 1: The one-loop quark self energy. The solid and dashed lines represent the quark and the scalar boson, respectively. 4-momenta  $P$  and  $K$  denote  $P = (\mathbf{p} = \mathbf{0}, \omega_m)$  and  $K = (\mathbf{k}, \omega_n)$ , respectively.

## II. YUKAWA MODEL COUPLED WITH A SCALAR BOSON

In this section, we formulate a Yukawa model with a massive quark and a massive scalar boson and evaluate the quark self-energy at one loop. The quark spectral function and some other quantities needed in the following sections are also introduced.

We start from the following Lagrangian composed of a quark and a scalar boson,

$$\mathcal{L} = \bar{\psi}(i\cancel{\partial} - m_f)\psi + \frac{1}{2}[(\partial_\mu\phi)^2 - m_b^2] - g\bar{\psi}\phi\psi, \quad (2.1)$$

with the quark mass  $m_f$ , the boson mass  $m_b$  and the coupling constant  $g$ . If the boson is a pseudoscalar,  $g$  should be replaced with  $i\gamma_5 g$ . This replacement may lead to non-trivial differences because the quarks are massive. The pseudoscalar case will be analyzed in Sec. V.

The spectral properties of the quark at zero momentum can be extracted from the retarded quark propagator

$$G^R(\omega) = [(\omega + i\eta) - m_f - \Sigma^R(\omega)]^{-1}, \quad (2.2)$$

with the retarded self-energy  $\Sigma^R(\omega)$ . We calculate the quark self-energy at finite  $T$  at one loop, which is diagrammatically shown in Fig. 1. In the imaginary-time formalism, it is given by

$$\tilde{\Sigma}(i\omega_m) = -g^2 T \sum_n \int \frac{d^3k}{(2\pi)^3} \mathcal{G}_0(\mathbf{k}, i\omega_n) \mathcal{D}(-\mathbf{k}, i\omega_m - i\omega_n), \quad (2.3)$$

where  $\mathcal{G}_0(\mathbf{k}, i\omega_n) = [i\omega_n \gamma^0 - \mathbf{k} \cdot \vec{\gamma} - m_f]^{-1}$  and  $\mathcal{D}(\mathbf{k}, i\nu_n) = [(i\nu_n)^2 - \mathbf{k}^2 - m_b^2]^{-1}$  are the Matsubara Green functions for the free quark and the free scalar boson, respectively, and  $\omega_n = (2n+1)\pi T$  and  $\nu_n = 2n\pi T$  are the Matsubara frequencies for fermions and bosons, respectively. Taking the summation over the Matsubara frequency and making the analytic continuation  $i\omega_n \rightarrow \omega + i\eta$ , one obtains the retarded self-energy  $\Sigma^R(\omega) = \tilde{\Sigma}(i\omega_n)|_{i\omega_n=\omega+i\eta}$ .

The self-energy  $\Sigma^R(\omega)$  has an ultraviolet divergence which originates from the  $T$ -independent part  $\Sigma_{T=0}^R(\omega) \equiv \lim_{T \rightarrow 0^+} \Sigma^R(\omega)$ . We remove this divergence by imposing the on-shell renormalization condition on the  $T$ -independent part of the quark propagator; for the details, see Appendix A. The  $T$ -dependent part,  $\Sigma_{T \neq 0}^R(\omega) \equiv \Sigma^R(\omega) - \Sigma_{T=0}^R(\omega)$ , on the other hand, is free from divergence [12]. For the numerical calculation, it is convenient

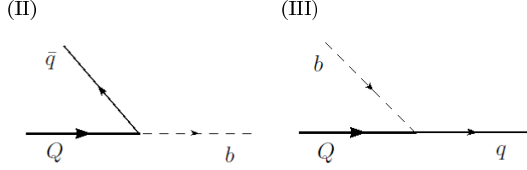


FIG. 2: The decay processes corresponding to the terms (II) and (III) in Eq. (2.8).

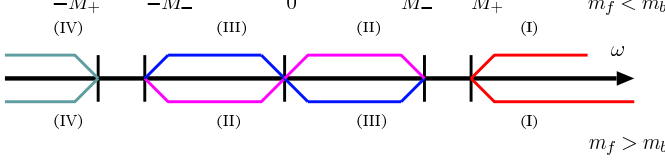


FIG. 3: The supports of the terms (I)-(IV) in Eq. (2.8). Here,  $M_+ \equiv m_b + m_f$  and  $M_- \equiv |m_b - m_f|$  are boundaries of the supports.

to first calculate  $\text{Im}\Sigma_{T \neq 0}^R(\omega)$  and then determine the real part via the Kramers-Kronig relation

$$\text{Re}\Sigma_{T \neq 0}^R(\omega) = \mathcal{P} \int_{-\infty}^{\infty} \frac{dz}{\pi} \frac{\text{Im}\Sigma_{T \neq 0}^R(z)}{z - \omega}, \quad (2.4)$$

where  $\mathcal{P}$  denotes the principal value.

The quark propagator for zero momentum is decomposed in the following way,

$$G^R(\omega) = G_+(\omega)\Lambda_+\gamma^0 + G_-(\omega)\Lambda_-\gamma^0, \quad (2.5)$$

with projection operators  $\Lambda_{\pm} \equiv (1 \pm \gamma^0)/2$  onto spinors whose chirality is equal(+) or opposite(-) to the helicity. We call +(-)-sector as ‘quark’(‘anti-quark’) sector. Here

$$\begin{aligned} G_{\pm}(\omega) &= \frac{1}{2} \text{Tr} [G^R(\omega)\gamma^0\Lambda_{\pm}] \\ &= [\omega + i\eta \mp m_f - \Sigma_{\pm}(\omega)]^{-1}, \end{aligned} \quad (2.6)$$

with  $\Sigma_{\pm}(\omega) = \text{tr}[\Sigma^R(\omega)\gamma^0\Lambda_{\pm}]$ . From the charge conjugation symmetry, we have a relation between  $G_{\pm}$  [3],

$$G_+(\omega) = -G_-^*(-\omega). \quad (2.7)$$

Because of this relation, we consider only the ‘quark’ sector  $G_+(\omega)$ . For  $m_f = 0$ , the propagator satisfies  $G_{\pm}(\omega) = -G_{\pm}^*(-\omega)$ . Notice that at finite quark number density, the charge conjugation symmetry is violated and Eq. (2.7) is no longer valid.

The imaginary part of  $\Sigma_+(\omega)$  is given by

$$\begin{aligned} \text{Im}\Sigma_+(\omega) &= -\frac{g^2}{2\pi} \int_0^{\infty} dk \frac{k^2}{E_k} \{ \\ &\quad \text{Tr}[\Lambda_+\Lambda_+(\mathbf{k})]\delta(\omega - E_f - E_b)[1 + n - f] \quad \text{(I)} \\ &\quad + \text{Tr}[\Lambda_+\Lambda_-(\mathbf{k})]\delta(\omega + E_f - E_b)[n + f] \quad \text{(II)} \\ &\quad + \text{Tr}[\Lambda_+\Lambda_+(\mathbf{k})]\delta(\omega - E_f + E_b)[n + f] \quad \text{(III)} \\ &\quad + \text{Tr}[\Lambda_+\Lambda_-(\mathbf{k})]\delta(\omega + E_f + E_b)[1 + n - f] \} \quad \text{(IV)}, \end{aligned} \quad (2.8)$$

where  $E_f = [m_f^2 + \mathbf{k}^2]^{1/2}$ ,  $E_b = [m_b^2 + \mathbf{k}^2]^{1/2}$ ,  $\Lambda_{\pm}(\mathbf{k}) = (E_f \pm \gamma^0(\vec{\gamma} \cdot \mathbf{k} + m_f))/(2E_f)$ , and  $f = (\exp(E_f/T) + 1)^{-1}$  and  $n = (\exp(E_b/T) - 1)^{-1}$  are the Fermi-Dirac and Bose-Einstein distribution functions, respectively. Equation (2.8) is proportional to the difference between the decay and creation rates of the quasi-quark. One can give a diagrammatical interpretation to each term (I)–(IV) [12, 13]. In Fig. 2, we show the decay processes included in the terms (II) and (III), which are called the Landau damping. The term (II) corresponds to a pair annihilation process between the quasi-quark ( $Q$ ) and a thermally excited anti-quark ( $\bar{q}$ ) with an emission of a boson ( $b$ ), and its inverse process. The term (III) corresponds to a scattering process of the quasi-quark by a thermally excited boson. The Landau damping vanishes at  $T = 0$ , as it involves thermally excited particles in the initial states. As we will see later, the Landau damping is enhanced rapidly as  $T$  goes high and plays a significant role for the peak structure in the quark spectrum.

Each term (I)–(IV) has a support on the  $\omega$  axis as shown in Fig. 3 owing to the energy-momentum conservation. While any value of  $\omega$  belongs to one support for  $m_f = 0$ , the ranges  $|m_b - m_f| < |\omega| < m_b + m_f$  are forbidden kinematically for  $m_f \neq 0$  and hence  $\text{Im}\Sigma_+(\omega) = 0$  there. In particular, the supports for the Landau damping (II) and (III) vanish for  $m_f = m_b$ .

The integral in Eq. (2.8) can be performed analytically to give

$$\begin{aligned} \text{Im}\Sigma_+(\omega) &= -\frac{g^2}{64\pi} \frac{(\omega + M_+)(\omega - M_-)}{\omega^3} \\ &\quad \times \sqrt{(\omega^2 - M_-^2)(\omega^2 - M_+^2)} \\ &\quad \times \left[ \coth \frac{\omega^2 + M_-M_+}{4\omega T} + \tanh \frac{\omega^2 - M_-M_+}{4\omega T} \right] \\ &\quad \times [\theta(\omega^2 - M_+^2) - \theta(M_-^2 - \omega^2)], \end{aligned} \quad (2.9)$$

where  $M_+ = m_f + m_b$ ,  $M_- = |m_b - m_f|$ , and  $\theta(\omega)$  is the step function.

In the following sections, we investigate the spectral properties of the quark by analyzing the spectral function and poles of the quark propagator. The spectral function is given by  $\rho(\omega) = -(1/\pi)\text{Im}G^R(\omega)$  which is decomposed, similarly to Eq. (2.5), as  $\rho(\omega) = \rho_+(\omega)\Lambda_+\gamma^0 + \rho_-(\omega)\Lambda_-\gamma^0$ , with

$$\begin{aligned} \rho_{\pm}(\omega) &= -\frac{1}{\pi} \text{Im}G_{\pm}(\omega) \\ &= -\frac{1}{\pi} \frac{\text{Im}\Sigma_{\pm}(\omega)}{(\omega \mp m_f - \text{Re}\Sigma_{\pm}(\omega))^2 + \text{Im}\Sigma_{\pm}(\omega)^2}. \end{aligned} \quad (2.10)$$

As directly derived from Eq. (2.7), the charge conjugation symmetry leads to

$$\rho_+(\omega) = \rho_-(-\omega). \quad (2.11)$$

In general,  $\rho_+(\omega)$  has several peaks corresponding to the quasi-quark excitations. Such excitations can also be expressed by complex poles of  $G_+(\omega)$  which are given by

solving

$$[G_+(z)]^{-1} = z - m_f - \Sigma_+(z) = 0, \quad (2.12)$$

with a complex number  $z$ . The causality requires that the solutions of Eq. (2.12) are in the lower-half complex-energy plane. The retarded self-energy  $\Sigma_+(z)$  in Eq. (2.12) for a lower-half complex-energy is given by

$$\Sigma_+(z) = \Sigma_+(\omega)|_{\omega \rightarrow z} + 2i [\text{Im}\Sigma_+(\omega)]_{\omega \rightarrow z}. \quad (2.13)$$

Notice that the analytic continuation of the retarded function to the lower-half plane requires the second term in Eq. (2.13) to compensate a cut of the first term on the real axis; for details of this analytic continuation, see Ref. [14]. The residue of each pole reads

$$Z = \left[ 1 - \frac{\partial \Sigma_+(z)}{\partial z} \right]^{-1}, \quad (2.14)$$

at the position of the pole  $z$ . We remark that the residue of a complex pole is a complex number in general.

To understand how the peak structure in  $\rho_+(\omega)$  emerges, it is also convenient to use the notion of “quasi-pole” which is defined as zero of the *real* part of the inverse propagator;

$$\omega - m_f - \text{Re}\Sigma_+(\omega) = 0. \quad (2.15)$$

Indeed, one sees from Eq. (2.10) that  $\rho_+(\omega)$  becomes large at  $\omega$  satisfying Eq. (2.15), provided that  $\text{Im}\Sigma_+(\omega)$  is small there.

### III. THE SPECTRAL FUNCTIONS OF QUARKS COUPLED WITH A SCALAR BOSON

In this section, we present the numerical results of the quark spectral function in the Yukawa model with a scalar boson. In order to see the effect of the quark mass  $m_f$ , we first recapitulate the result for  $m_f = 0$  [12], focusing on its  $T$ -dependence at zero momentum. We then show the numerical results for massive quarks. The behavior of the self-energy is also analyzed for both cases. We fix the coupling constant  $g$  unity throughout this and subsequent sections. We have checked that our results do not change qualitatively with the variation of  $g$  over a rather wide range [12].

#### A. Quark spectrum with $m_f = 0$

In the left upper panel of Fig. 4, we show the  $T$ -dependence of the spectral function  $\rho_+(\omega)$  with  $m_f = 0$ .  $\rho_+(\omega)$  takes on a peak with a  $\delta$ -function shape at the origin independently of  $T$ . In this figure, the height of this peak denotes  $Z \times 10$  with  $Z$  being the residue of the corresponding pole in the quark propagator. At  $T = 0$ , the residue is unity owing to the on-shell renormalization

condition. As  $T$  is raised, the magnitude of the present residue decreases while two bumps newly appear at finite energies and eventually turn to narrow peaks. At intermediate temperatures, i.e.,  $\tau \equiv T/m_b = 1-1.5$ ,  $\rho_+(\omega)$  thus has a three-peak structure [11, 12]. As will be shown in the next section, there exist poles corresponding to the new two peaks, and the residues of the three poles tend to have almost the same magnitude in this range of  $T$ , which indicates that the three peaks are equally significant. As  $T$  is raised further, the residue of the pole at the origin damps quickly and  $\rho_+(\omega)$  is dominated by the two peaks at finite energies: These two peaks can be identified with the normal quasi-quark and the anti-plasmino excitations [12] which are familiar collective fermion excitations obtained in the HTL approximation in gauge theories [3]. The positions of these peaks correspond to the thermal masses.

To understand the  $T$ -dependence of  $\rho_+(\omega)$ , we analyze the imaginary and real parts of  $\Sigma_+(\omega)$ , which are shown in Fig. 5. For  $m_f = 0$ , the self-energy  $\Sigma_+(\omega)$  has symmetry properties,  $\text{Im}\Sigma_+(\omega) = \text{Im}\Sigma_+(-\omega)$  and  $\text{Re}\Sigma_+(\omega) = -\text{Re}\Sigma_+(-\omega)$ . At  $T = 0$ ,  $\text{Im}\Sigma_+(\omega)$  takes non-zero values only for  $|\omega| > m_b$  corresponding to the supports of the terms (I) and (IV) in Eq. (2.8). At  $T \neq 0$ ,  $\text{Im}\Sigma_+(\omega)$  gets to have a support in the region  $|\omega| < m_b$  owing to the Landau damping, i.e. the terms (II) and (III), and forms two peaks there. The heights of these peaks grow up quickly as  $T$  is raised.

Then owing to the Kramers-Kronig relation between the real and imaginary parts of the self-energy Eq. (2.4),  $\text{Re}\Sigma_+(\omega)$  inevitably shows a steep rise in the two regions of  $\omega$  corresponding to the peak regions of  $\text{Im}\Sigma_+(\omega)$  for  $|\omega| < m_b$  [12]; their steepness and the magnitudes are amplified as  $T$  is raised.

This oscillatory behavior of  $\text{Re}\Sigma_+(\omega)$  affects the number of quasi-poles. In the lower panel of Fig. 5, we show a line  $\text{Re}\Sigma_+(\omega) = \omega$  to find the solutions of Eq. (2.15); crossing points between this line and  $\text{Re}\Sigma_+(\omega)$  give the quasi-poles. The figure shows that at low  $T$ , there exists only one quasi-pole at the origin. As  $T$  is raised, the oscillatory behavior of  $\text{Re}\Sigma_+(\omega)$  is so enhanced that four new quasi-poles get to exist. However,  $\text{Im}\Sigma_+(\omega)$  has so large values at two of the quasi-poles that any peak structure in  $\rho_+(\omega)$  is not formed at these points; thus we end up with only the three peaks in the spectral function at the origin and the other two quasi-poles where  $\text{Im}\Sigma_+(\omega)$  is small. The moral which one should learn from the above discussion is that the Landau damping which causes two peaks in  $\text{Im}\Sigma_+(\omega)$  is essential for the formation of the three-peak structure in  $\rho_+(\omega)$ ; see Appendix B for an elucidating discussion with use of an analytic toy model for the self-energy.

#### B. Quark spectral function with small quark mass

In this subsection, we investigate how a finite but small quark mass affects and modifies the quark spectral func-

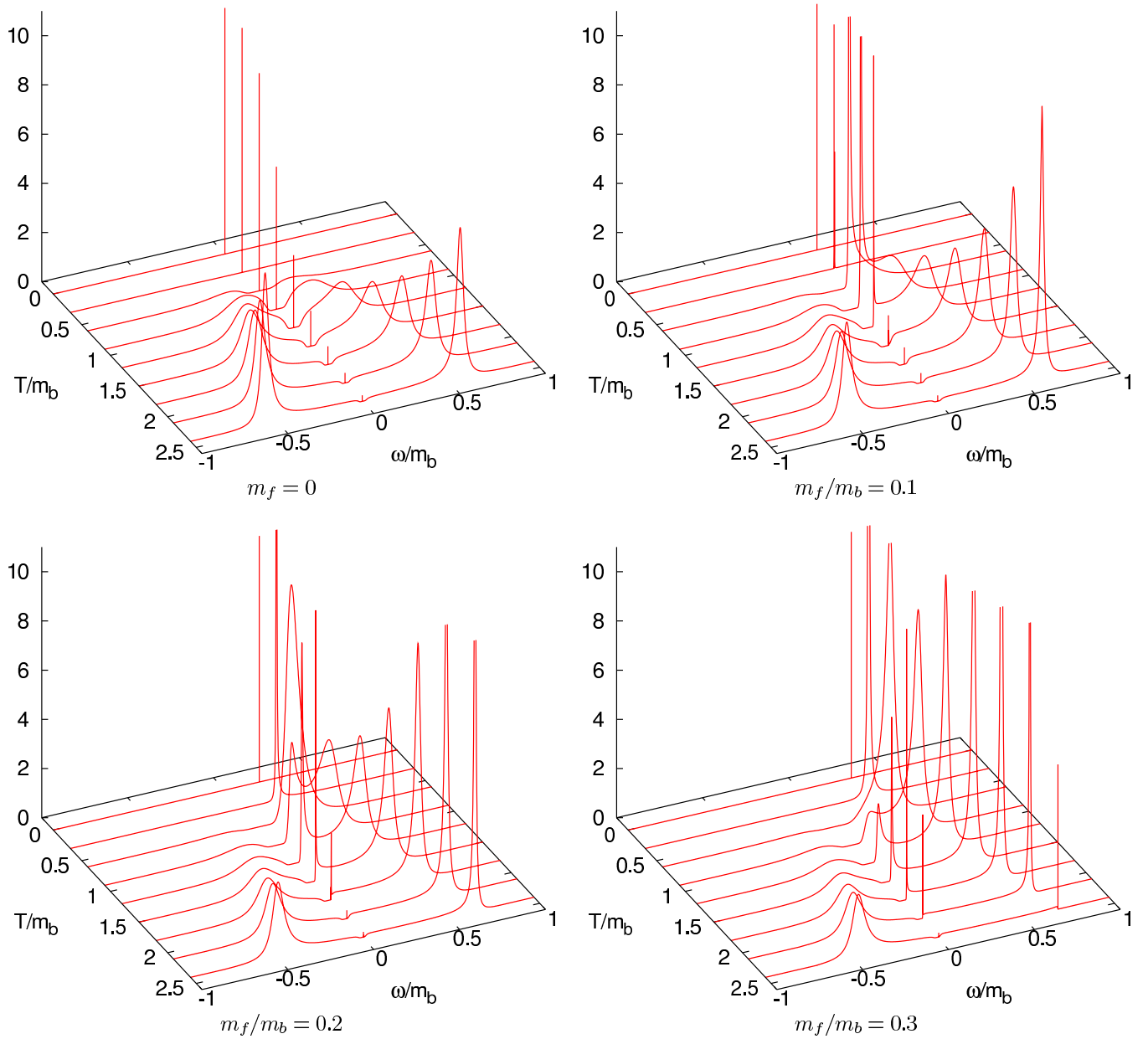


FIG. 4: The quark spectral functions  $m_b \rho_+(\omega)$  for  $m_f/m_b = 0, 0.1, 0.2$  and  $0.3$ . The heights of the peaks of the  $\delta$ -function shape represent  $Z \times 10$  with  $Z$  being the residue.

tion  $\rho_+(\omega)$ .

We show  $\rho_+(\omega)$  with  $m_f/m_b = 0.1$  in the upper-right panel of Fig. 4. At  $T = 0$ ,  $\rho_+(\omega)$  takes on a peak with a  $\delta$ -function shape at  $\omega = m_f$ ; this pole always exists in  $\rho_+(\omega)$  at  $T = 0$  irrespective of the value of  $m_f$ . As  $T$  is raised, this peak gets to have a width and moves toward the origin. There also appears a shoulder in the positive-energy region larger than  $m_f$ , which turns to a narrow peak at  $\tau \equiv T/m_b \gtrsim 1.5$ . In the negative-energy region, there appears also another peak whose development is slower than that in the positive energy region. The three-peak structure is then barely seen in  $\rho_+(\omega)$  at  $\tau \simeq 1$ .

In the lower-left panel of Fig. 4, we show the spectral functions for  $m_f/m_b = 0.2$ . As mentioned above, there exists a peak of the  $\delta$ -function type at  $\omega = m_f$  at  $T = 0$ . As  $T$  is raised, this peak becomes broader and eventually splits into two peaks; one of which approaches the origin while the other connects to the normal quasi-quark excitation having a non-zero thermal mass at high  $T$ . There also appears a broad bump in the negative-energy region, which only gradually gets developed into a peak at higher  $T$  than that in the positive-energy region. Thus, the number of clear peaks in  $\rho_+(\omega)$  at a certain  $T$  is two at most, and a clear three-peak structure is hardly seen.

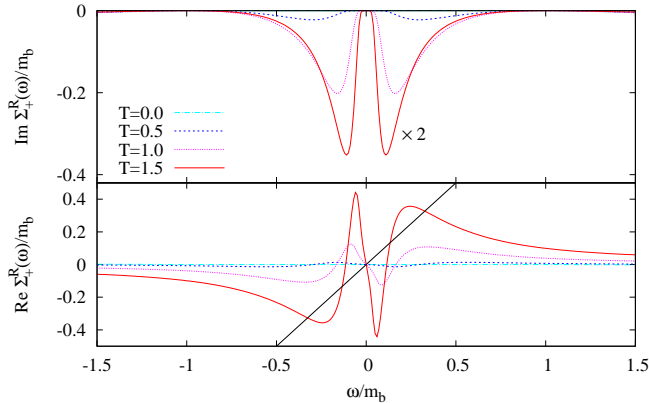


FIG. 5: The quark self-energy  $\Sigma_+(\omega)$  with  $m_f = 0$  for  $T/m_b = 0, 0.5, 1.0$  and  $1.5$ . The upper and lower panels show the imaginary and real parts, respectively.

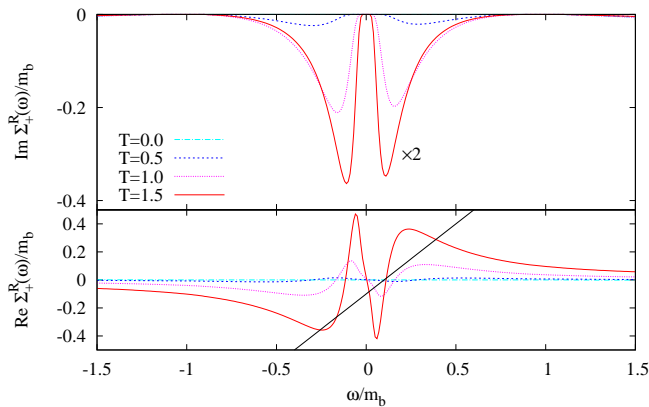


FIG. 6: The quark self-energy  $\Sigma_+(\omega)$  with  $m_f/m_b = 0.2$  for several values of  $T$ .

In the lower-right panel of Fig. 4, the spectral function  $\rho_+$  for  $m_f/m_b = 0.3$  is shown. We see that the peak at  $\omega = m_f$  at  $T = 0$  smoothly connects to the normal quasi-quark excitation in the high  $T$  limit, which is quite different from the cases with  $m_f/m_b \leq 0.2$ . Furthermore, the three-peak structure in  $\rho_+(\omega)$  does not appear for any  $T$ ; this is because the peak in the negative-energy region develops only very slowly with increasing  $T$ . As we will see later in Sec. IV, this behavior reflects in the  $T$ -dependence of the poles of the quark propagator. This qualitative change of the  $T$ -dependence of the pole behaviors can be understood in terms of the level crossing as will be discussed in Sec. VI.

The effects of  $m_f$  on the behavior of  $\rho_+(\omega)$  can be understood more precisely by analyzing the  $m_f$ -dependence of the self-energy and quasi-poles. In Fig. 6, we show

$\Sigma_+(\omega)$  for  $m_f/m_b = 0.2$ . Comparing this figure with Fig. 5, one finds that the behavior of  $\Sigma_+(\omega)$  hardly changes with this slight change of the quark mass. Since the quasi-poles are given by solving  $\text{Re}\Sigma_+(\omega) = \omega - m_f$ , the dominant effect of  $m_f$  thus comes from the quark mass term in the r.h.s. of the above equation. The line to determine the solutions of this equation is shifted lower with  $m_f \neq 0$ , as shown in Fig. 6. Owing to this shift, there arises an asymmetry in the positions of quasi-poles in positive- and negative-energy regions. The two quasi-poles in the positive-energy region emerge at lower temperature, while the quasi-pole in the negative-energy region at higher temperature.

#### IV. THE POLE STRUCTURE OF QUARK COUPLED WITH SCALAR BOSON

In this section, we investigate the pole structure of the quark propagator  $G_+(\omega)$ . We find the three poles which correspond to the peaks in  $\rho_+(\omega)$  discussed in the previous section, and analyze their  $T$ -dependence. It is found that the  $T$ -dependence of the poles shows a drastic change at  $m_f/m_b \simeq 0.21$ , which means that the physics contents of the collective quark excitations are changed at this point.

##### A. Pole structure of massless quark

We first examine the case with  $m_f = 0$ . The poles of the quark propagator are given as complex roots of Eq. (2.12).

We first notice that  $G_+(z)$  has an infinite number of poles in the lower-half complex-energy plane. In particular, there are two series of infinite poles near the imaginary axis whose density increases infinitely as they approach the origin. The manifestation of these poles is mathematically attributed to the hyperbolic cotangent and tangent in Eq. (2.9),

$$\coth\left(\frac{z^2 + m_b^2}{4zT}\right) + \tanh\left(\frac{z^2 - m_b^2}{4zT}\right), \quad (4.1)$$

where we have set  $m_f = 0$ . For  $m_b \neq 0$ , the arguments of them diverge as  $\sim 1/z$  at the origin, and these terms lead to a rapid oscillation of  $\Sigma_+(z)$  in the complex-energy plane. On the imaginary axis, for example, this term behaves as  $\cot(1/\zeta) + \tan(1/\zeta)$  near the origin with  $\zeta = -iz$ , and thus  $\text{Im}\Sigma_+(\zeta)$  has infinite number of divergences around the origin. This behavior also brings about singularities of  $\text{Re}\Sigma_+(\zeta)$  through the Kramers-Kronig relation Eq. (2.4), and leads to the infinite number of roots of Eq. (2.12) near the imaginary axis. These poles, however, do not correspond to any peaks in the spectral function, and thus has no physical significance. Because this oscillation comes from the  $T$ -dependent term, this is specific at finite  $T$ .

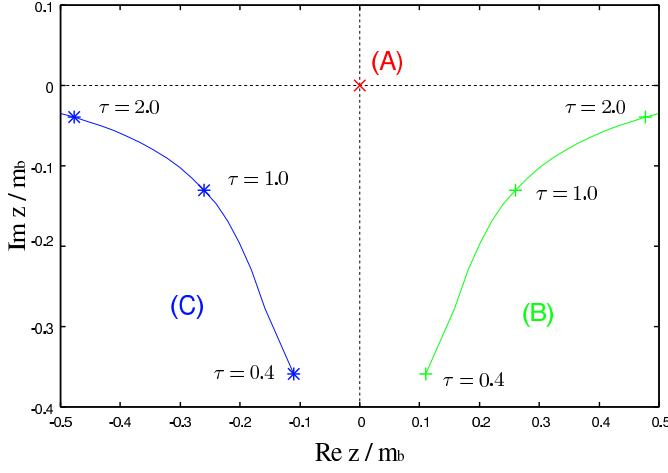


FIG. 7: The  $T$ -dependence of the poles (A)–(C) with  $m_f = 0$ .

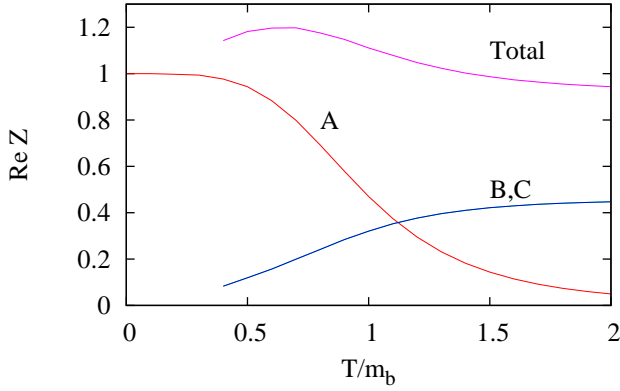


FIG. 8: The  $T$ -dependence of  $\text{Re}Z$  of the poles (A)–(C) with  $m_f = 0$ . The summation of  $\text{Re}Z$ , Eq. (4.4), is also shown.

Besides these poles, we have found that there exist isolated three poles which have a physical significance in the sense that they all correspond to the peaks in  $\rho_+(\omega)$ . One of them is that existing at the origin independently of  $T$ . We label this pole as (A) in the following. For  $\tau \gtrsim 2.0$ , we find the other two poles associated with the sharp peaks in  $\rho_+(\omega)$ ; one has a positive real part and is labeled as (B), while the other has a negative real part and is labeled as (C). As  $T$  is lowered, the poles (B) and (C) move toward the region containing the above-mentioned infinite poles and become hard to distinguish from them numerically: For  $\tau < 0.4$ , our numerical algorithm failed to identify these two poles, and the pole search is stopped at  $\tau = 0.4$ . In the following, we concentrate on the poles (A)–(C), since they have physical significance: Indeed it will be shown that the peak structure of  $G_+(\omega)$  is well described solely by these three poles.

In Fig. 7, we show the  $T$ -dependence of the positions

of the poles (A)–(C). The real parts of the residues at these poles,  $\text{Re}Z_A$ ,  $\text{Re}Z_B$  and  $\text{Re}Z_C$ , are also shown in Fig. 8. One sees from these figures that for relatively low  $T$ ,  $|\text{Im}z_B|$  and  $|\text{Im}z_C|$  are large and  $\text{Re}Z_B$  and  $\text{Re}Z_C$  are small, which is consistent with the result in the previous section that  $\rho_+(\omega)$  is dominated by the pole (A) at sufficiently low  $T$ . For  $\tau \simeq 1.2$ , all the residues have the same value, which indicates that the collective excitations corresponding to these three poles have a similar strength. For high temperatures,  $|\text{Im}z_B|$  and  $|\text{Im}z_C|$  become smaller in accordance with the formation of the sharp peaks in  $\rho_+(\omega)$ .

In order to check that the poles (A)–(C) certainly correspond to the peaks in  $\rho_+(\omega)$ , we compare the spectral function with that constructed from a Breit-Wigner (BW) approximation

$$\rho_+^{\text{BW}}(\omega) = -\frac{1}{\pi} \text{Im} \sum_{i=A,B,C} \frac{Z_i}{\omega - z_i}. \quad (4.2)$$

This approximated and the original spectral functions for  $\tau = 0.5, 1$  and  $1.5$  are plotted in the upper panels of Fig. 9. One sees that  $\rho_+^{\text{BW}}(\omega)$  well reproduces the original spectral function  $\rho_+(\omega)$ , especially for higher  $T$ . We thus conclude that the three poles well represent the excitation property of the quasi-quark. The BW approximation, however, fails to reproduce the precise shape of  $\rho_+(\omega)$  around the origin, which is due to the contributions of the infinite series of poles near the imaginary axis.

The fermion spectral function satisfies the sum rule

$$\int_{-\infty}^{\infty} d\omega \rho_+(\omega) = 1. \quad (4.3)$$

If the poles (A)–(C) well describe the whole analytic structure of the propagator, the sum of the residues  $\sum_i Z_i$  should take a value close to unity, provided that a possible violation of the sum rule owing to a renormalization procedure is negligible [3].

Here, we first notice that, with the BW approximation Eq. (4.2), the left hand side of Eq. (4.3) is given by,

$$\int_{-\infty}^{\infty} d\omega \rho_+^{\text{BW}}(\omega) = \sum_{i=A,B,C} \text{Re}Z_i \equiv Z_{\text{Tot}}, \quad (4.4)$$

which tells us that only the real part of the residue contributes to the strength of the spectrum. The  $T$  dependence of  $Z_{\text{Tot}}$  as well as  $\text{Re}Z_i$  ( $i = A, B$  and  $C$ ) are shown in Fig. 8. One sees that the sum  $Z_{\text{Tot}}$  gives a value close to unity in the whole range of  $T$  with a small deviation, about 20% at most. We remark that if the values of residues of the infinite series of poles around the imaginary axis is added to  $Z_{\text{Tot}}$  the deviation from unity becomes much smaller.

Finally, we examine the poles (A)–(C) for  $\tau \gg 1$ . In Fig. 10, we show the poles (A)–(C) up to  $\tau \simeq 40$ . The poles (B) and (C) reach the real axis at  $\omega = m_b$  when  $\tau \simeq 4.2$ . This is due to a suppression of the phase space of the decay processes at  $\omega = m_b$ . For higher  $T$ ,  $|\text{Im}z/m_b|$



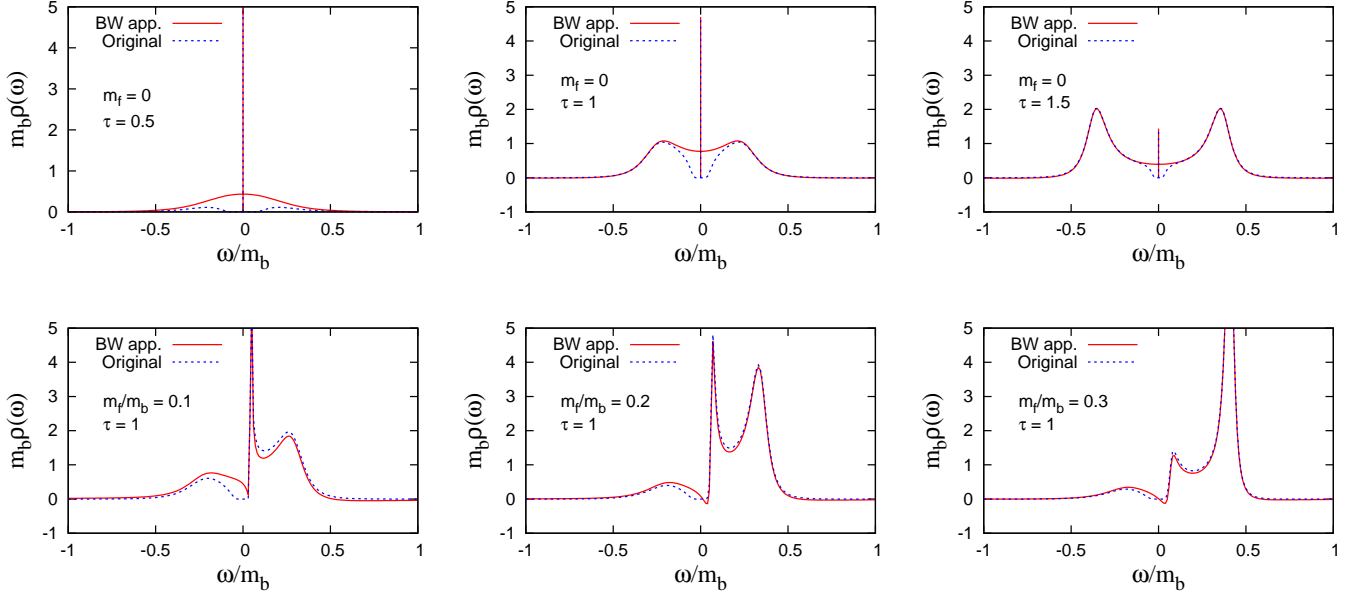


FIG. 9: The comparison of the spectral functions with the Breit-Wigner approximations  $\rho_+^{\text{BW}}(\omega)$  and the original one  $\rho_+(\omega)$  for several quark masses and temperatures.

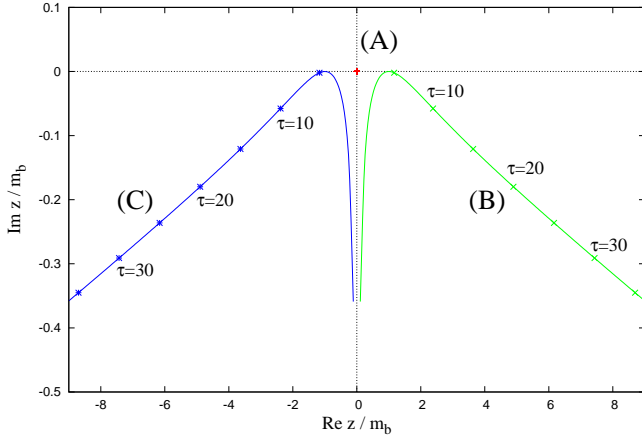


FIG. 10: The  $T$ -dependence of the poles (A)–(C) with  $m_f = 0$  up to  $\tau \simeq 40$ . The points denote the position of poles for  $\tau = 5, 10, 15, \dots$ .

for the poles (B) and (C) increase monotonically with  $T$ . At sufficiently high  $T$ , the real parts of the poles (B) and (C) take a value close to those determined in the HTL approximation having the thermal mass  $m_T = gT/4$  [12], although there is a small deviation owing to the strong coupling  $g = 1$  taken here. The behavior of the imaginary part of each pole is also consistent with that in the HTL approximation which gives the width of order  $gm_T$  [3]. Although there always exists the pole (A) at the origin, the residue of this pole decreases and becomes negligible in the high- $T$  limit.

## B. Pole structure of massive quark

In this subsection, we examine the  $T$ -dependence of the pole structure of the propagator for the massive quarks by varying the quark mass ( $m_f/m_b = 0.1 \rightarrow 0.3$ ). We shall show how the small but non-vanishing quark mass significantly affects the physics contents of the quasi-quark excitations at finite  $T$ .

First of all, we have found that there exist the three poles of physical significance which correspond to a peak or bump in the spectral function even for the massive quarks, too: The lower panels of Fig. 9, show the spectral functions in the BW approximation  $\rho_+^{\text{BW}}(\omega)$  for  $m_f/m_b = 0.1, 0.2$  and  $0.3$  with fixed  $\tau = 1$ . We see that the BW approximation solely with the three poles well reproduces the original spectral functions even for the cases of massive quarks, which means that the three poles well represent the physical excitations of quarks even with finite  $m_f$ . Here we mention that an infinite number of poles due to a kinematical origin exist also for finite  $m_f$  around the imaginary axis as in the case of  $m_f = 0$ .

We show the  $T$  dependence of the poles for  $m_f/m_b = 0.1$  in Fig. 11. The figure shows that the pole (A) moves toward the origin as  $T$  is raised, while the poles (B) and (C) move toward the real axis almost symmetrically with respect to the imaginary axis: The small asymmetry of the two trajectories is caused by the fact that  $|\text{Im} z_B|$  is always smaller than  $|\text{Im} z_C|$  in the range of  $\tau$  shown in the figure. This inequality for the imaginary parts is consistent with the behavior of  $\rho_+(\omega)$  that the peak in the positive-energy region is sharper than that in the negative-energy one. In Fig. 12, we show  $\text{Re} z_i$  of each



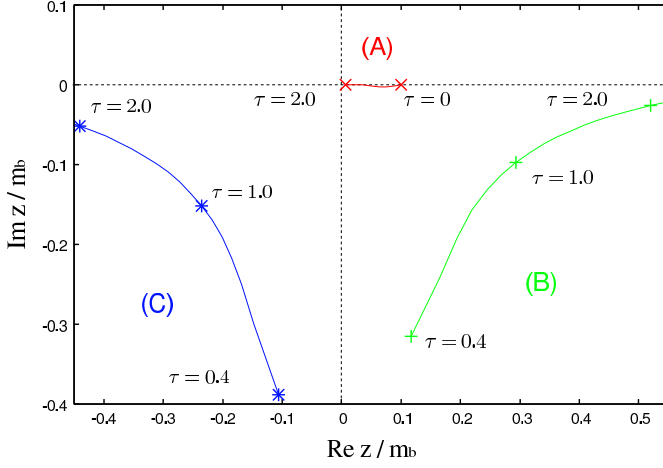


FIG. 11: The  $T$ -dependence of the poles (A)~(C) with  $m_f = 0.1$ .

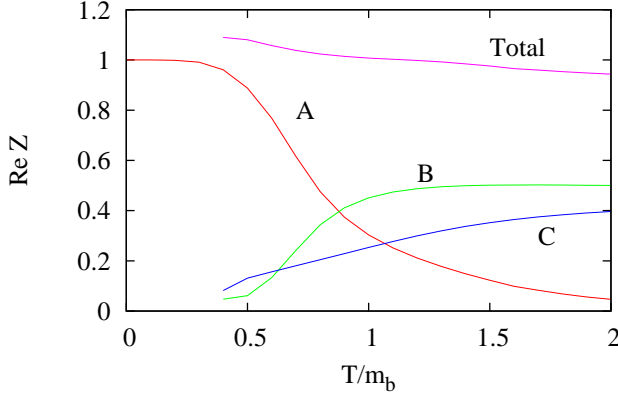


FIG. 12: The  $T$ -dependence of  $\text{Re}Z$  with  $m_f = 0.1$ .

pole in the case of  $m_f/m_b = 0.1$ . The  $T$ -dependence of each residue is qualitatively the same as that for  $m_f = 0$ . We notice that the residues for all the poles have similar values at  $\tau \simeq 1$  where a three-peak structure is barely seen in  $\rho_+(\omega)$ . For temperatures much higher than those shown in Fig. 11, the poles (B) and (C) eventually reach the real axis at  $|\text{Re}z_{B,C}| = m_b - m_f$ . As  $T$  rises further, they move on the real axis until  $|\text{Re}z_{B,C}| = m_b + m_f$  at which the poles start to leave the real axis. This movement of the poles along the real axis for some temperatures reflects the support structure of the  $\text{Im}\Sigma_+(\omega)$  as shown in Fig. 3. For  $\tau \gg 1$ , the positions of the poles approach those for  $m_f = 0$  shown in Fig. 10.

Let us turn to the case with  $m_f/m_b = 0.2$ . The  $T$ -dependence of the poles in this case is shown in Figs. 13: Although the topology of the set of the trajectories and the behaviors of the poles along with the variation of  $T$  are qualitatively the same as before, a notable point is that the trajectories of the poles (A) and (B) are so

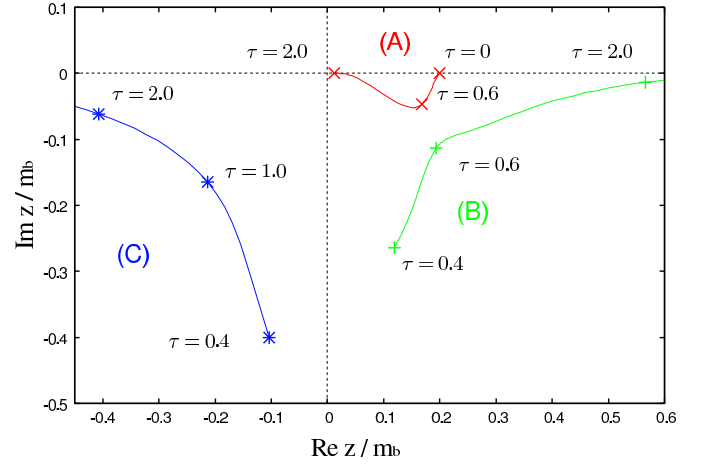


FIG. 13: The  $T$ -dependence of the poles (A)~(C) with  $m_f/m_b = 0.2$ .

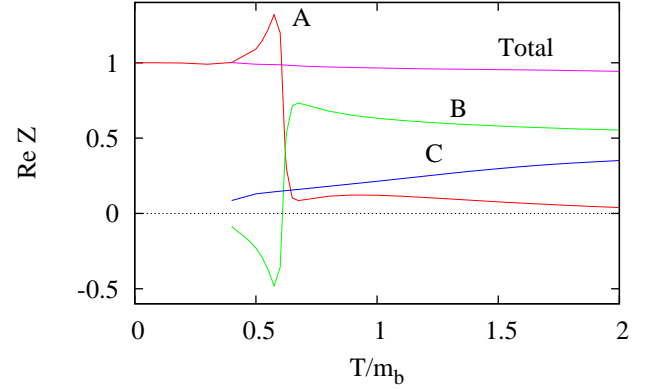


FIG. 14: The  $T$ -dependence of  $\text{Re}Z$  with  $m_f/m_b = 0.2$ .

deformed that they tend to get close to each other around  $\tau = 0.6$ . As we will see later, this is actually a precursory deformation leading to a structural rearrangement of the trajectories to be seen for the larger  $m_f/m_b$ .

The  $T$ -dependence of the pole residues  $\text{Re}Z_i$  ( $i = A, B, C$ ) is shown in Fig. 14. We see that the behavior of them are quite different from those for smaller quark masses: As  $T$  is raised,  $\text{Re}Z_A$  first increases and then rapidly drops at  $\tau \simeq 0.6$ , while  $\text{Re}Z_B$  behaves oppositely. The sum of the residues  $Z_{\text{Tot}}$  is, however, almost unity for any  $T$ . It should be noted that although  $\text{Re}Z_B$  is negative around  $\tau = 0.6$ , the pole (B) does not correspond to any peak in the spectral function nor hence describe a physical excitation.

Finally let us examine the case with  $m_f/m_b = 0.3$ . Fig. 15 shows how the three poles move along with the increase of  $T$ . At a first glance, one can see that a drastic change has occurred by a small increase of  $m_f/m_b$

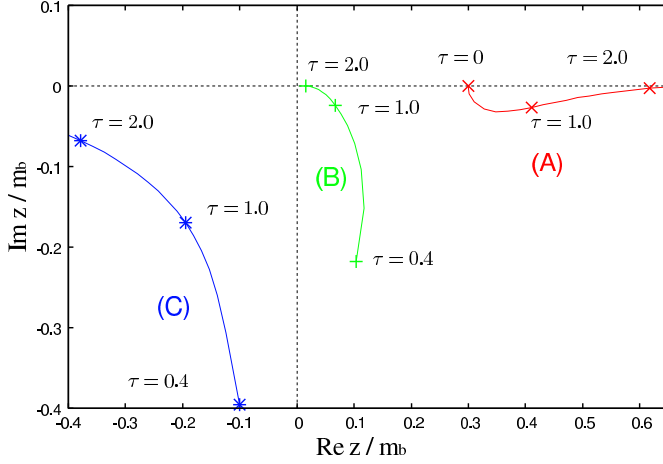


FIG. 15: The  $T$ -dependence of the poles (A)–(C) with  $m_f/m_b = 0.3$ .

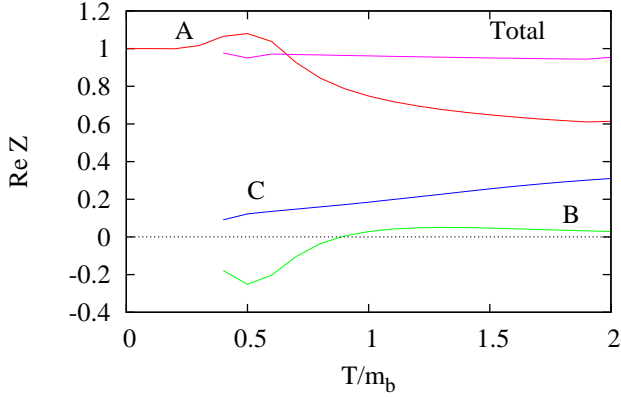


FIG. 16: The  $T$ -dependence of  $\text{Re}z$  of the poles (A)–(C) with  $m_f/m_b = 0.3$ .

from 0.2 in the topology of the set of the three trajectories as well as in the  $T$ -dependence of the poles. The pole (A), which is identified as one smoothly connecting to  $\omega = m_f$  at  $T = 0$ , moves with increasing  $T$  toward large positive energies with a small or vanishing imaginary part, as pole (B) did in the previous cases, instead of going to the origin as the pole (A) did before. On the other hand, the pole (B) first appears with a large imaginary part near the imaginary axis at  $\tau = 0.4$  and tends to move toward the real axis at high temperatures as in the cases of  $m_f/m_b \leq 0.2$ , but then changes the direction and approaches the origin as  $T$  is raised further, as the pole (A) did in the previous cases. We now see that the poles (A) and (B) at high temperatures has exchanged their characters with each other; this exchange should have occurred at a critical quark mass  $m_{fc}$  which is located between  $0.2m_b$  and  $0.3m_b$ . The character exchange

of the poles is a kind of level crossing familiar in Quantum mechanics. In geometrical terms, when  $m_f = m_{fc}$ , the trajectories of pole (A) and (B) are so deformed that the two trajectories would touch each other at some temperature ( $\tau \sim 0.6$ ), and then for larger quark masses than  $m_{fc}$ , the two trajectories would be rearranged to form trajectories as shown in Fig. 15. Indeed, we have numerically confirmed that the trajectories of the poles (A) and (B) get close to and then touch each other eventually at  $m_f/m_b \simeq 0.21$ , i.e.,  $m_{fc} \simeq 0.2m_b$ . The  $T$ -dependence of  $\text{Re}z$  of each pole for  $m_f/m_b = 0.3$ , shown in Fig. 16, can also be understood naturally with the notion of the level crossing.

## V. SPECTRAL PROPERTIES OF QUARKS COUPLED WITH PSEUDOSCALAR BOSONS

In this section, we replace the scalar boson with a pseudoscalar one and investigate how the behavior of the spectral function and the pole structure change. Throughout this section, we put a superscript “PS” to all the functions where PS is for pseudoscalar boson. When we refer to the functions calculated in the previous sections, we put a superscript “S” where S is for scalar boson.

The Lagrangian density of the Yukawa model composed of a quark and a pseudoscalar boson is given by,

$$\mathcal{L}_{\text{PS}} = \bar{\psi}(i\partial\!\!\!/ - m_f)\psi + \frac{1}{2}[(\partial_\mu\phi)^2 - m_b^2] - g\bar{\psi}(i\gamma_5\phi)\psi. \quad (5.1)$$

The quark self-energy in this model in the imaginary time formalism at one loop reads

$$\tilde{\Sigma}^{\text{PS}}(i\omega_m) = -g^2T \sum_n \int \frac{d^3k}{(2\pi)^3} i\gamma_5 \mathcal{G}_0(\mathbf{k}, i\omega_n) \times i\gamma_5 \mathcal{D}(-\mathbf{k}, i\omega_m - i\omega_n). \quad (5.2)$$

The difference between Eqs. (5.2) and (2.3) is the two factors of  $i\gamma_5$  only. As one can easily check, this difference leads to the following simple relations for the retarded self-energies,

$$\text{Re}\Sigma_+^{\text{PS}}(\omega) = -\text{Re}\Sigma_+^{\text{S}}(-\omega), \quad (5.3)$$

$$\text{Im}\Sigma_+^{\text{PS}}(\omega) = \text{Im}\Sigma_+^{\text{S}}(-\omega). \quad (5.4)$$

For  $m_f = 0$ , one immediately obtains  $\Sigma_+^{\text{PS}}(\omega) = \Sigma_+^{\text{S}}(\omega)$ , and thereby the type of bosons does not affect the quark propagator at all [12] in accordance with the chiral symmetry.

In Fig. 17, we show the imaginary and real parts of the self-energy with the scalar and the pseudoscalar bosons for  $m_f/m_b = 0.3$  and  $\tau = 1.5$ . We see that the behavior of them is qualitatively the same as that for the scalar boson.

From this feature, one naturally expects that the resulting spectral function and the pole structure are also insensitive to the type of the boson. In Fig. 18, we show

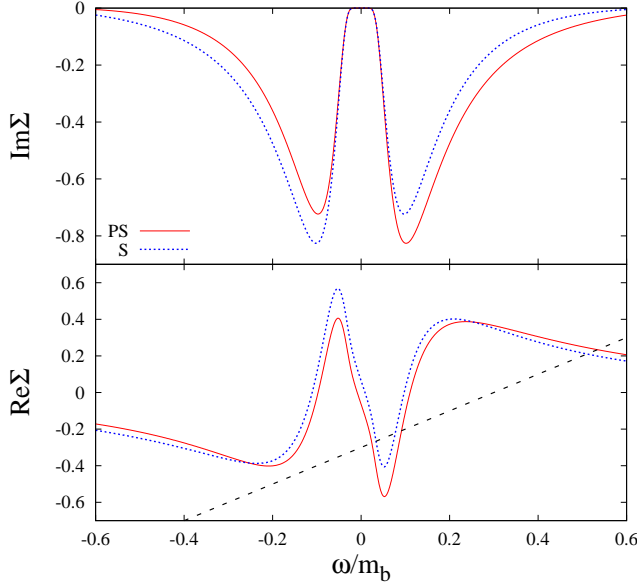


FIG. 17: The imaginary and real parts of the self-energies  $\Sigma^S(\omega)$  and  $\Sigma^{PS}(\omega)$  for  $m_f/m_b = 0.3$  at  $\tau = 1.5$ . The dashed line is the line  $\omega - m_f$ .

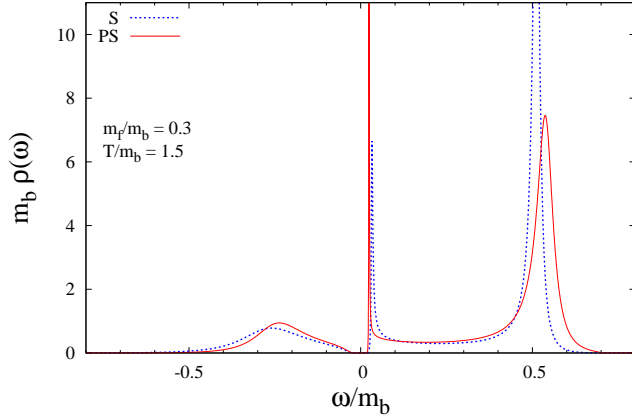


FIG. 18: The comparison of the spectral functions of the quark coupled with the scalar and pseudoscalar bosons. The labels “S” and “PS” stand for the scalar and pseudoscalar bosons, respectively.

the spectral functions  $\rho_+^{PS}(\omega)$  and  $\rho_+^S(\omega)$  for  $m_f/m_b = 0.3$  and  $\tau = 1.5$ . One sees that the peak structures of these spectral functions are qualitatively the same, indeed. The pole position is shown in Fig. 19 for  $m_f/m_b = 0.2$  and  $0.3$ . We find again that each pole behaves similarly as before. Quantitatively,  $|\text{Im}z_A|$  is always smaller than that obtained in the previous section, while  $|\text{Im}z_B|$  is larger. The level crossing between the poles (A) and

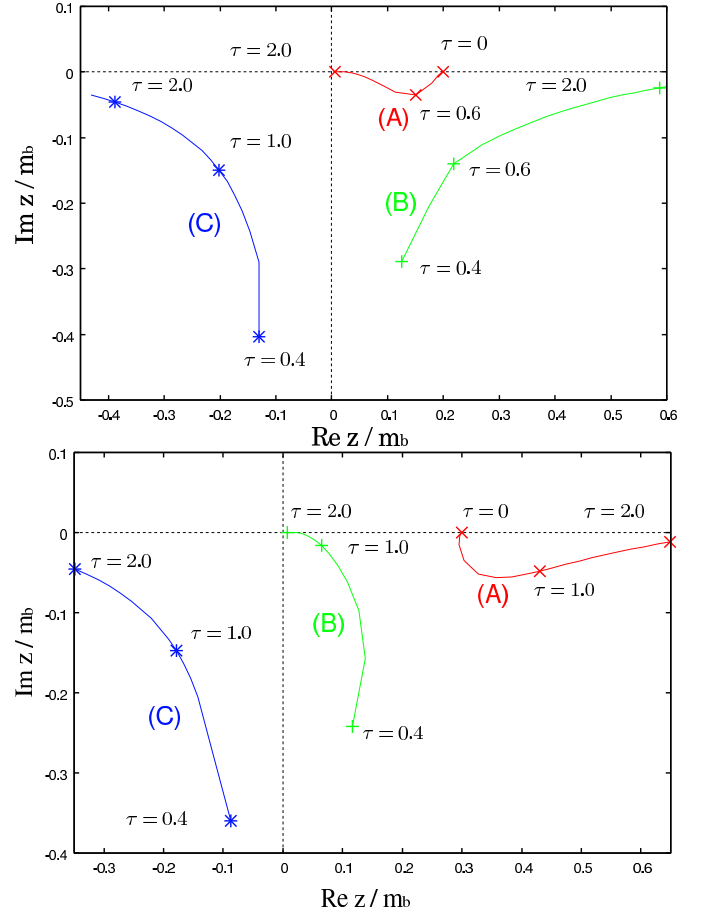


FIG. 19: The  $T$ -dependence of the poles. The upper and lower panels are for  $m_f/m_b = 0.2$  and  $0.3$ , respectively.

(B) occurs for this case also at  $m_f/m_b \simeq 0.23$ , which is slightly larger than that for the scalar boson.

## VI. DISCUSSIONS; LEVEL MIXING INDUCED BY RESONANT SCATTERING

In the preceding sections, we have studied the spectral properties of quarks coupled with scalar and pseudoscalar bosons by examining the spectral function  $\rho_+(\omega)$  and the pole structure of the quark propagator. We have found that, although the three-peak structure for  $m_f = 0$  survives even for finite  $m_f$ , such structure gradually ceases to exist and the number of clear poles in  $\rho_+(\omega)$  becomes two at most for  $m_f/m_b \gtrsim 0.2$ . The behavior of  $\rho_+(\omega)$  and the position of poles at finite  $m_f$  show a drastic change as if there is a level crossing at  $m_f/m_b \simeq 0.21$  ( $0.23$ ) when coupled with a scalar (pseudoscalar) boson. In this section, we elucidate the mechanism for realizing this behavior in terms of the notion of the so called resonant scattering [15].

We first recall that the formation of two peaks in  $\text{Im}\Sigma_+^R(\omega)$  plays a decisive role to cause the three-peak structure in  $\rho_+(\omega)$  (See, Sec. III and App. B.). The de-

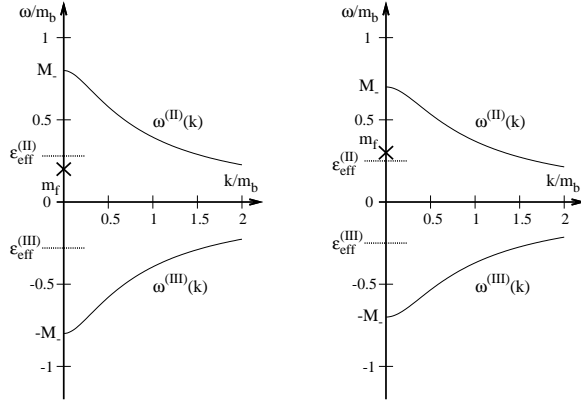


FIG. 20: The energy levels for  $m_f/m_b = 0.2$  (left) and  $0.3$  (right). The solid lines are  $\omega^{(II)}(k)$  for  $\omega > 0$  and  $\omega^{(III)}(k)$  for  $\omega < 0$ . The crosses indicate the free-quark energy at zero momentum,  $\omega = m_f$ . The dashed lines  $\varepsilon_{\text{eff}}^{(II)}$  and  $\varepsilon_{\text{eff}}^{(III)}$  denote the most probable energy levels of  $\omega^{(II)}(k)$  and  $\omega^{(III)}(k)$ , respectively..

cay rates corresponding to these two peaks are due to the Landau damping, which is diagrammatically depicted in Fig. 2: The term (II) is the pair annihilation process of the quasi-quark ( $Q$ ) and a thermally excited anti-quark ( $\bar{q}$ ) into a boson  $b$ ,  $Q + \bar{q} \rightarrow b$ , and its inverse process. Here, we notice that the annihilation of a thermally excited anti-quark can be regarded as the creation of a hole with a positive quark number in the anti-quark distribution. With this interpretation, the term (II) is schematically described as  $Q \rightarrow \bar{q}^{\text{hole}} + b$ ; the quasi-quark is converted to a hole in the anti-quark distribution with an emission of a boson. The term (III) is schematically depicted as  $Q + b \rightarrow q$ . This process has a support for  $\omega < 0$  and the quasi-quark  $Q$  is dominated by hole components of anti-quarks in this energy range. Through the process of the term (III), the quasi-quark is converted to the on-shell quark, and thus the mixing between a quark and a hole of anti-quark is induced.

Scattering processes of a boson would induce a mixing between particle and hole states at finite  $T$ , which are called the resonant scattering [11, 12, 15]. The resonant scattering causes a level repulsion in the energy spectra of the fermionic excitations. In the case of superconducting phase transition, for example, the preformed-pair modes induce a resonant scattering between particle and hole states in the Fermi sea; the outcome is a gap-like structure around the Fermi surface, i.e., the so called *pseudogap*, in the fermion spectral function [15]. For the chiral phase transition, it was shown [11, 12] that a resonant scattering between a quark and an anti-quark hole is induced through the coupling with the chiral soft modes; there appears a three-peak structure in the quark spectral function  $\rho_+(\omega)$  in the low-energy and low-momentum region [11], see, Eqs. (3.18) and (3.19) in Ref. [12].

Now, let us consider the level mixing for the present case with  $m_f \neq 0$ . We first focus on the term (II) with the energy conservation

$$\omega_Q = -E_f(-\mathbf{k}) + E_b(\mathbf{k}) \equiv \omega^{(II)}(k), \quad (6.1)$$

with  $k = |\mathbf{k}|$ , where  $\omega_Q$  is the energy of the quasi-quark  $Q$  with zero momentum.  $\omega^{(II)}(k)$  denotes the energy of the two-particle state composed of a boson with momentum  $\mathbf{k}$  and an antiquark-hole with momentum  $-\mathbf{k}$ , and is varied with  $k$  from  $M_- = m_b - m_f$  to 0 as shown by the solid lines in Fig. 20. Although  $\omega^{(II)}(k)$  can take any value between 0 and  $M_-$ , there exists a value where the process corresponding to (II) is most probable. Such a value may be given by the peak position of  $\text{Im}\Sigma_+^S(\omega^{(II)}(k))$  due to the term (II). We denote the peak position as  $\varepsilon_{\text{eff}}^{(II)}$  and show it in Fig. 20. Then, the physical energy spectrum at zero momentum is realized effectively through a level repulsion between  $\varepsilon_{\text{eff}}^{(II)}$  and the on-shell free-quark energy  $m_f$ . From Fig. 20, one finds that  $\varepsilon_{\text{eff}}^{(II)}$  gets to exceed  $m_f$  at a mass between  $m_f/m_b = 0.2$  and  $0.3$  when  $m_f$  is increased. This crossover is also seen from the movement of the peak position of  $\text{Im}\Sigma_+^S(\omega)$  relative to  $m_f$ , as shown in Fig. 21: For  $m_f/m_b = 0.1$  and  $0.2$ ,  $\varepsilon_{\text{eff}}^{(II)}$  is larger than  $m_f$ , while for  $m_f/m_b = 0.3$ ,  $\varepsilon_{\text{eff}}^{(II)}$  becomes smaller than  $m_f$ . Now, when  $\varepsilon_{\text{eff}}^{(II)} > m_f$ , which is the case for  $m_f/m_b < 0.21$ , the state with the unperturbed energy  $m_f$  tends to have a lower energy than  $m_f$ , while that with  $\varepsilon_{\text{eff}}^{(II)}$  to have higher energy than  $\varepsilon_{\text{eff}}^{(II)}$  by the coupling through the resonant scattering with the boson. On the other hand, when  $\varepsilon_{\text{eff}}^{(II)} < m_f$ , as is the case for  $m_f/m_b > 0.21$ , the state with the unperturbed energy  $m_f$  tends to have a higher energy than  $m_f$ , while that with  $\varepsilon_{\text{eff}}^{(II)}$  to have lower than  $\varepsilon_{\text{eff}}^{(II)}$ . Thus we have seen that the level-crossing phenomenon between poles (A) and (B) or the trajectory rearrangement at  $m_f/m_b \simeq 0.21$  can be nicely account for in terms of the level repulsion induced by the resonant scattering.

Similar discussions hold for the process of the term (III), where the energy conservation reads

$$\omega_Q = E_f(-\mathbf{k}) - E_b(\mathbf{k}) \equiv \omega^{(III)}(k). \quad (6.2)$$

$\omega^{(III)}(k)$  is drawn in Fig. 20 with a solid line in the negative energy region. The most probable energy,  $\varepsilon_{\text{eff}}^{(III)}$ , in this case is then negative, and thus  $\varepsilon_{\text{eff}}^{(III)} < m_f$  is satisfied irrespective of the value of  $m_f$ . The physical energy spectrum at zero momentum is again obtained effectively as a result of the level repulsion between  $\varepsilon_{\text{eff}}^{(III)}$  and  $m_f$ . Because  $\varepsilon_{\text{eff}}^{(III)}$  and  $m_f$  never cross, there is no qualitative change in the  $T$ -dependence of the pole (C) unlike the process of the term (II): The real part of the position of the pole (C) monotonically decreases as  $\tau$  increases, as shown in Figs. 11, 13 and 15. As  $m_f/m_b$  increases with  $\tau$  fixed,  $\varepsilon_{\text{eff}}^{(III)}$  goes farther from  $m_f$ , which means that

the effect of the level repulsion gets weaker and thus the strength of the pole (C) gets weaker, as shown in Fig. 4.

We thus find that the  $T$ -dependence of the poles in the quark propagator for each  $m_f$  can be understood in terms of the level repulsion which is induced by a resonant scattering of the massive boson with a quark and an anti-quark hole.

## VII. SUMMARY AND DISCUSSION

In this paper, we have investigated the spectral properties of quarks with a Dirac mass  $m_f$  coupled with a scalar and pseudoscalar boson with a mass  $m_b$  at finite temperature ( $T$ ). We have employed Yukawa models to describe the system and studied the spectral function and the pole structure of the quark propagator for zero momentum at one loop. The spectral function in the same models at finite  $T$  was studied for the case with  $m_f = 0$  in Ref. [12], where the formation of the three-peak structure was observed at intermediate temperature  $T/m_b \simeq 1$ . In the present study, we have examined effects of  $m_f$  on the spectral function in the range  $m_f/m_b < 0.3$  focusing on the spectral properties at zero momentum. It was found that, although the three-peak structure found in Ref. [12] survives with finite  $m_f$ , it tends to be suppressed as  $m_f/m_b$  becomes larger. We showed that the  $T$  dependence of the free pole at  $\omega = m_f$  changes qualitatively as  $m_f/m_b$  becomes larger.

We have newly investigated the pole structure of the retarded quark propagator in the lower-half complex-energy plane and the residues. Our numerical calculation has identified the three poles corresponding to the peaks in the spectral function, although near the imaginary axis, there are infinite number of poles which do not form peaks in the spectral function. The  $T$ -dependence of the three poles is consistent with that of the corresponding peaks in the spectral function. We have found that the  $T$ -dependence of the poles changes qualitatively around  $m_f/m_b \simeq 0.21$  (0.23) for Yukawa models with scalar (pseudoscalar) boson. This behavior is consistent with the behavior of the spectral function and suggests that the physical contents of the collective quark excitations at finite  $T$  change qualitatively around this value of the quark mass. We have given an interpretation for this characteristic change of the collective excitations in terms of the level crossing induced by the resonant scattering [11, 12].

The spectral function in the Yukawa model at finite  $T$  was studied in Ref. [13], for the case with  $m_b = 0$ . In this case, the spectral function gradually changes between a single- and two-peak structures as  $T/m_b$  is varied as an external parameter. It is an interesting project to explore the pole structure in this case, and the possible qualitative change of them in the whole region of parameters  $m_f$ ,  $m_b$  and  $T$ . This result will be reported elsewhere.

The present study has a relevance to the study of effects of hadronic excitations [8, 10] in the QGP phase

on the quasi-particle picture of the quark. One of the plausible candidates of such a hadronic mode is the soft modes of the chiral transition [8] since they can become light near  $T_c$ . The effect of the soft modes on the quark spectrum has been considered in Ref. [11] in the chiral effective model in the chiral limit. In this case, the quarks are massless above  $T_c$  and the soft modes become massless at  $T_c$ . If the chiral symmetry is explicitly broken, on the other hand, the chiral phase transition at finite  $T$  becomes crossover and the quarks have a finite mass for any value of  $T$  [16]. The soft modes do not become massless, either. These effects would suppress the formation of the three-peak structure in the quark spectrum near  $T_c$ , as we have seen in the analysis of the present work. The masses of quarks and soft modes, however, varies dynamically as functions of  $T$  in the QGP phase. In order to investigate the effect of the soft modes more quantitatively, the study of the quark spectrum with a chiral model incorporating the explicit chiral symmetry breaking is desirable.

The quark spectral function near but above  $T_c$  is recently analyzed in quenched lattice QCD in Ref. [6], where the quark spectral function  $\rho_+(\omega)$  at zero momentum is analyzed as a function of  $m_f$ . It is shown that  $\rho_+(\omega)$  is well described by a two-pole ansatz. This result means that the three-peak structure is hardly formed in the quark spectrum in quenched QCD. We note, however, that the effect of the hadronic excitations is not incorporated in the quenched approximation. The full lattice simulation would properly describe the effect of such excitations on the quark spectrum.

It is an interesting problem to explore the effect of the multi-peak structure on experimental observables. For example, the dilepton production rate is an interesting candidate which can be affected by the structure of the quark propagator [17]. The excitation spectrum at low energy may modify the thermodynamic quantities, such as the transport coefficients. To examine these observables with the quark propagator obtained in the present study is beyond the scope of this work and left as a future project.

Since the model which we have employed in this work is a simple but generic Yukawa model with a massive boson, the results can be applied to various systems at finite  $T$  composed of a massive fermion and a massive boson. For example, the quark spectrum might have a multi-peak structure through couplings with massive bosonic states instead of the soft modes, such as glueballs, charmonia, and so on. Another example is the excitation spectra of neutrinos coupled with weak bosons at  $T$  near the masses of the weak bosons [18]. The multi-peak spectral function of a Dirac particle with a vanishing or small mass might be realized in some two-dimensional materials such as graphene [19] and an organic conductor  $\alpha$ -(BEDT-TTF)<sub>2</sub>I<sub>3</sub> salt [20] which exhibit Dirac-type dispersion relations.

We are grateful to Berndt Muller, Kenji Fukushima and the members of Hadron-Quark Seminar in Kyoto

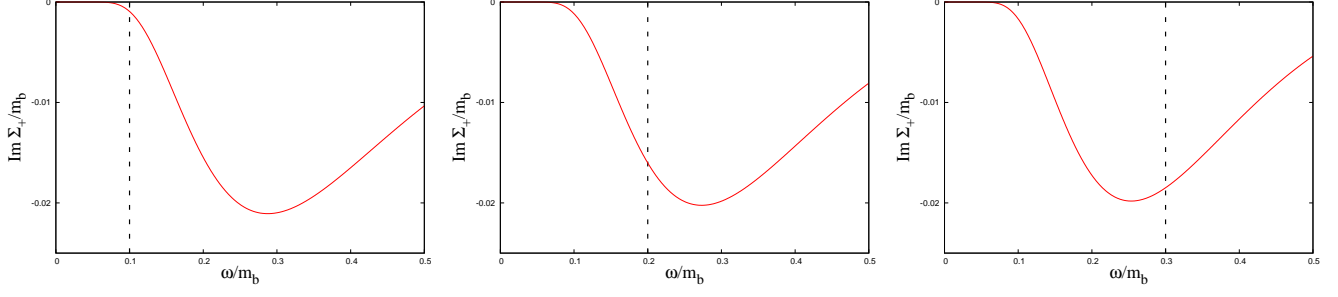


FIG. 21: The imaginary part of the quark self-energy  $\text{Im}\Sigma_+^S(\omega)$  for  $m_f/m_b = 0.1, 0.2$  and  $0.3$  with fixed  $\tau = 0.5$ . The dotted lines represent  $\omega = m_f$ .  $\tau$  is chosen as the value at which  $\rho_+(\omega)$  and the position of pole (A) start to show a clear deviation from those for  $T = 0$ .

University for their interest and encouragement. M. K. is supported by a Grant-in-Aid for Scientific Research by Monbu-Kagakusyo of Japan (No. 19840037). T. K. is supported by a Grant-in-Aid for Scientific Research by Monbu-Kagakusyo of Japan (No. 17540250). Y. N. is supported by a JSPS Grant-in-Aid for Scientific Research (#18740140). This work is supported by the Grant-in-Aid for the 21st Century COE “Center for Diversity and Universality in Physics” of Kyoto University. The numerical calculations were carried out on Altix3700 BX2 at YITP in Kyoto University.

## APPENDIX A: RENORMALIZATION OF THE $T$ -INDEPENDENT PART OF THE QUARK PROPAGATOR

In this appendix, we calculate the  $T$ -independent part of the quark self-energy  $\Sigma_{T=0}^R(\omega)$ , which has an ultraviolet divergence. The renormalization is carried out using the subtracted dispersion relation. In the following, we concentrate on the quark part  $\Sigma_{+,T=0}(\omega)$ , because the anti-quark part  $\Sigma_{-,T=0}(\omega)$  can be dealt with in the same way.

We first note that  $\text{Im}\Sigma_{+,T=0}$  is free from divergence and thus can be calculated without regularization. Taking a limit  $T \rightarrow 0^+$  in Eq. (2.8), one obtains

$$\text{Im}\Sigma_{+,T=0}(\omega) = -\frac{g^2}{32\pi} \frac{(\omega - M_-)(\omega + M_+)}{\omega^3} S(\omega) \epsilon_\omega \theta(\omega^2 - M_+^2), \quad (\text{A1})$$

where  $M_- = m_b - m_f$ ,  $M_+ = m_b + m_f$ ,  $S(\omega) = \sqrt{(\omega^2 - M_-^2)(\omega^2 - M_+^2)}$ ,  $\epsilon_\omega = \omega/|\omega|$  is the sign of  $\omega$  and  $\theta(\omega)$  is the step function.

To determine the real part  $\text{Re}\Sigma_{+,T=0}(\omega)$ , we use the

subtracted dispersion relation

$$\begin{aligned} \text{Re}\Sigma_{+,T=0}(\omega) &= \sum_{l=0}^{n-1} \frac{(\omega - \alpha)^l}{l!} c_l \\ &+ \frac{(\omega - \alpha)^n}{\pi} \mathcal{P} \int_{-\infty}^{\infty} d\zeta \frac{\text{Im}\Sigma_{+,T=0}^R(\zeta)}{(\zeta - \omega)(\zeta - \alpha)^n}, \end{aligned} \quad (\text{A2})$$

where  $\alpha$  denotes the renormalization point,  $c_l$  are the subtraction constants, and  $n$  is the number of subtraction. To regularize the ultraviolet divergence, we use Eq. (A2) with  $n = 2$ .

The subtraction constants  $c_0$  and  $c_1$  may be determined by the on-shell renormalization conditions for the mass and the wave function at  $\alpha = m_f$ , which are tantamount to requiring that

$$\Sigma_{+,T=0}(m_f) = 0, \quad (\text{A3})$$

and

$$\left. \frac{\partial \Sigma_{+,T=0}(\omega)}{\partial \omega} \right|_{\omega=m_f} = 0, \quad (\text{A4})$$

respectively. From Eqs. (A3) and (A4), we obtain  $c_0 = c_1 = 0$ , and then the renormalization is completed.

## APPENDIX B: GENERIC NATURE OF THE THREE-PEAK STRUCTURE IN THE QUARK SPECTRUM; AN ANALYTIC TOY MODEL

We have seen in the main text and Refs. [11, 12] that the two-peak structure in the imaginary part of the quark self-energy leads to the three-peak structure in the quark spectral function. In this appendix, we show that this has a generic nature using a simple but generic model. For simplicity, we consider the case for vanishing momentum as in the main text.

First, let us consider the quark spectrum for the massless quark. To investigate effects of the peak structure in the imaginary part of the self-energy on the quark spectrum, we assume that the imaginary part of the retarded

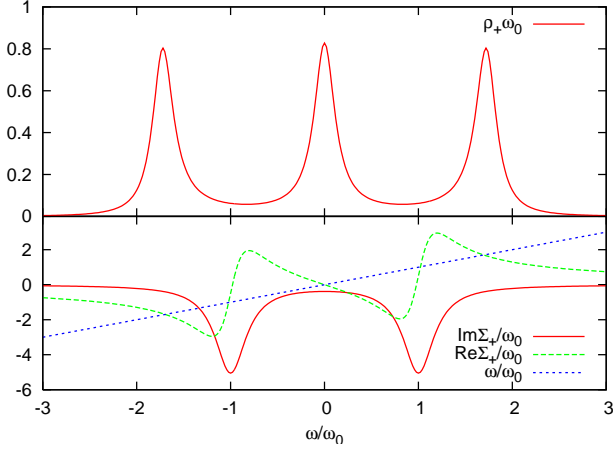


FIG. 22: The spectral function  $\rho_+$  and the self-energy  $\Sigma_+$  for  $\gamma/\omega_0 = 0.2$ . The quark mass is taken to be zero.

quark self-energy consists of two peaks expressed with Lorentzian forms,

$$\text{Im}\Sigma_+(\omega) = -M^2 \left[ \frac{\gamma_1}{(\omega_1 - \omega)^2 + \gamma_1^2} + \frac{\gamma_2}{(\omega_2 - \omega)^2 + \gamma_2^2} \right], \quad (\text{B1})$$

where  $\omega_{1,2}$  denote the peak positions and  $\gamma_{1,2}$  denote the widths. An overall factor  $M^2$  having mass dimension two is put because the quark self-energy has mass dimension one. Since we are interested in the number of peaks in the quark spectrum, the deviation of the peak shape from the Lorentzian form is not important here. For the massless quark, we have  $\omega_0 \equiv \omega_1 = -\omega_2$  and  $\gamma \equiv \gamma_1 = \gamma_2$  from a symmetry property of the self-energy. As discussed in the main text and Refs. [11, 12], the formation of the peaks in  $\text{Im}\Sigma_+$  is caused by the Landau damping which is scattering processes with a boson. As  $T$  increases, the peaks become higher rapidly as shown in Figs. 5 and 6, which corresponds to  $\gamma/\omega_0$  being smaller.

The corresponding real part of the self-energy is uniquely determined from the imaginary part: Because the Landau damping is a medium effect, the real part is ultraviolet finite and given by the un-subtracted dispersion relation,

$$\begin{aligned} \text{Re}\Sigma_+(\omega) &= \mathcal{P} \int_{-\infty}^{\infty} \frac{d\omega'}{\pi} \frac{\text{Im}\Sigma_+(\omega')}{\omega' - \omega} \\ &= M^2 \left[ \frac{\omega - \omega_0}{(\omega_0 - \omega)^2 + \gamma^2} + \frac{\omega + \omega_0}{(\omega_0 + \omega)^2 + \gamma^2} \right]. \end{aligned} \quad (\text{B2})$$

The spectral function is then obtained from the self-energy,  $\rho_+(\omega) = -1/\pi \cdot \text{Im}\Sigma_+(\omega)/[(\omega - \text{Re}\Sigma_+(\omega))^2 + \text{Im}\Sigma_+(\omega)^2]$ .

As an example, we plot the spectral function and the self-energy for  $\gamma/\omega_0 = 0.2$  in Fig. 22. For simplicity, we have set  $M = \omega_0$ . From the number of crossing points between  $\text{Re}\Sigma_+$  and the line  $\omega/\omega_0$ , one finds that this self-energy is close to that for  $T = 1.5$  shown in Fig. 5. We

see that the resultant quark spectral function  $\rho_+$  has a clear three-peak structure. For smaller values of  $\gamma/\omega_0$ , i.e. higher  $T$ , the three peaks are sharper and higher than those in Fig. 22.

For very high  $T$ , however, the strength of the central peak in  $\rho_+$  gets weaker and eventually  $\rho_+$  becomes to have only two peaks which correspond to the normal quasi-quark and the anti-plasmino as shown in Fig. 4. In the Yukawa models, this can be understood from the fact that as  $T$  increases, in addition to two peaks in  $\text{Im}\Sigma_+$  being higher, the positions of the two peaks approaches the origin. In terms of Eq. (B1), this means  $\omega_1/T, \omega_2/T \rightarrow 0$  for  $T \rightarrow \infty$ , thus it becomes hard to distinguish the two peaks, and thus  $\text{Im}\Sigma_+$  only shows a one-peak structure as a whole. One can show in a generic way that the one-peak structure of  $\text{Im}\Sigma_+$  leads to a two-peak structure of the quark spectral function. In fact, this rule can be extended to the cases where  $\text{Im}\Sigma_+$  has multiple peaks; the number of the peaks in  $\text{Im}\Sigma_+$  is significantly reflected in the number of the peaks in  $\rho_+$ .

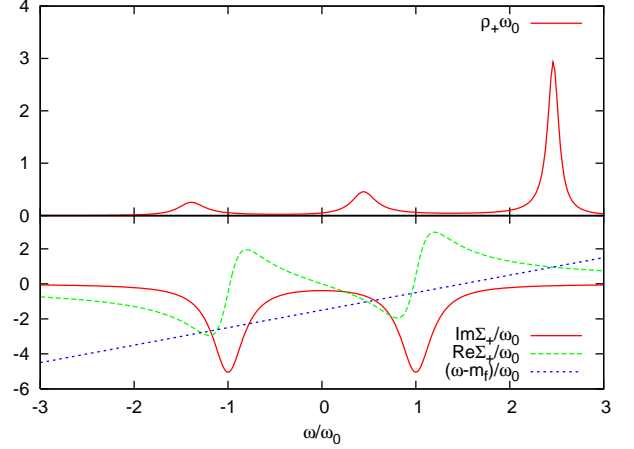


FIG. 23: The spectral function  $\rho_+$  and the self-energy  $\Sigma_+$  for  $\gamma/\omega_0 = 0.2$  and  $m_f/\omega_0 = 1.5$ .

Next we consider the quark spectrum for the massive quark. In this case,  $\omega_1$  and  $\gamma_1$  are in general not identical to  $-\omega_2$  and  $\gamma_2$ , respectively. However, from Fig. 6, we see that such asymmetry is not so large for small values of the quark mass  $m_f$ . Then, for simplicity, we employ the same self-energy as that for the massless quark. The mass effect only enters the expression of the spectral function,  $\rho_+(\omega) = -1/\pi \cdot \text{Im}\Sigma_+(\omega)/[(\omega - m_f - \text{Re}\Sigma_+(\omega))^2 + \text{Im}\Sigma_+(\omega)^2]$ .

As an example, we plot the spectral function and the self-energy for  $\gamma/\omega_0 = 0.2$  and  $m_f/\omega_0 = 1.5$  in Fig. 23. From the number of crossing points between  $\text{Re}\Sigma_+$  and the line  $(\omega - m_f)/\omega_0$ , this self-energy is close to that for  $T = 1.5$  in Fig. 6. We see that the rightmost peak is enhanced, which results from the shift of the crossing points. This result of the quark spectrum is also consistent with that in Fig. 4.



For very high  $T$ , the effect of the quark mass becomes relatively smaller and thus the quark spectrum approaches that for the massless quark mentioned above.

In short, we have shown that a simple but plausible as-

sumption on the peak structure in the imaginary part of the self-energy generically leads to the multi-peak structure in the quark spectral function obtained in dynamical models such as the Yukawa models.

- 
- [1] R. D. Pisarski, Phys. Rev. Lett. **63**, 1129 (1989); E. Braaten and R. D. Pisarski, Nucl. Phys. **B337**, 569 (1990); *ibid*, **B339**, 310 (1990).
  - [2] V.V. Klimov, Sov. J. Nucl. Phys. **33**, 934 (1981) [Yad. Fiz. **33** (1981), 1734]; H.A. Weldon, Phys. Rev. D **28**, 2007 (1983).
  - [3] See, for example, M. Le Bellac, *Thermal Field Theory* (Cambridge University Press, Cambridge, England 1996).
  - [4] I. Arsene *et al.* [BRAHMS Collaboration], Nucl. Phys. A **757**, 1 (2005). B. B. Back *et al.*, Nucl. Phys. A **757**, 28 (2005); J. Adams *et al.* [STAR Collaboration], Nucl. Phys. A **757**, 102 (2005); K. Adcox *et al.* [PHENIX Collaboration], Nucl. Phys. A **757**, 184 (2005).
  - [5] R. J. Fries, B. Muller, C. Nonaka and S. A. Bass, Phys. Rev. Lett. **90**, 202303 (2003); Phys. Rev. C **68**, 044902 (2003); V. Greco, C. M. Ko and P. Levai, Phys. Rev. Lett. **90**, 202302 (2003); S. A. Voloshin, Nucl. Phys. A **715**, 379 (2003); D. Molnar and S. A. Voloshin, Phys. Rev. Lett. **91**, 092301 (2003).
  - [6] F. Karsch and M. Kitazawa, Phys. Lett. B **658**, 45 (2007).
  - [7] M. Harada, Y. Nemoto and S. Yoshimoto, arXiv:0708.3351 [hep-ph].
  - [8] T. Hatsuda and T. Kunihiro, Phys. Lett. B **145**, 7 (1984); Phys. Rev. Lett. **55** (1985) 158.
  - [9] T. Matsui and H. Satz, Phys. Lett. B **178**, 416 (1986).
  - [10] M. Asakawa and T. Hatsuda, Phys. Rev. Lett. **92**, 012001 (2004); S. Datta, F. Karsch, P. Petreczky and I. Wetzorke, Phys. Rev. D **69**, 094507 (2004); T. Umeda, K. Nomura and H. Matsufuru, Eur. Phys. J. C **39S1**, 9 (2005); H. Iida, T. Doi, N. Ishii, H. Suganuma and K. Tsumura, Phys. Rev. D **74**, 074502 (2006); A. Jakovác, P. Petreczky, K. Petrov and A. Velytsky, Phys. Rev. D **75**, 014506 (2007). G. Aarts, C. Allton, M. B. Oktay, M. Peardon and J. I. Skullerud, Phys. Rev. D **76**, 094513 (2007).
  - [11] M. Kitazawa, T. Kunihiro and Y. Nemoto, Phys. Lett. B **633**, 269 (2006); see also, arXiv:hep-ph/0510381.
  - [12] M. Kitazawa, T. Kunihiro and Y. Nemoto, Prog. Theor. Phys. **117**, 103 (2007).
  - [13] G. Baym, J. P. Blaizot and B. Svetitsky, Phys. Rev. D **46**, 4043 (1992).
  - [14] see e.g. appendix B in, M. Kitazawa, T. Koide, T. Kunihiro and Y. Nemoto, Prog. Theor. Phys. **114**, 205 (2005).
  - [15] B. Janko, J. Maly and K. Levin, Phys. Rev. B **56**, R11407 (1997); M. Kitazawa, T. Kunihiro and Y. Nemoto, Phys. Lett. B **631**, 157 (2005).
  - [16] S. P. Klevansky, Rev. Mod. Phys. **64**, 649 (1992); T. Hatsuda and T. Kunihiro, Phys. Rept. **247**, 221 (1994).
  - [17] E. Braaten, R. D. Pisarski and T. C. Yuan, Phys. Rev. Lett. **64**, 2242 (1990).
  - [18] D. Boyanovsky, Phys. Rev. D **72**, 033004 (2005).
  - [19] K. S. Novoselov *et al.*, Nature **438**, 197 (2005); Y. Zhang *et al* Nature **438**, 201 (2005).  
Interesting physical problems related to graphene may be seen from a special issue of Nature Materials **6** NO.3, (2007).
  - [20] S. Katayama, A. Kobayashi and Y. Suzumura, J. Phys. Soc. Jpn, **75**, 054705 (2006).